



Contents lists available at ScienceDirect

Arabian Journal of Chemistry

journal homepage: www.ksu.edu.sa

Enhanced mechanical strength of micro-porous ceramics through the removal of alkaline earth carbonates from Moroccan red clay for membrane support application

Yassine Rakcho^{a,*}, Mossaab Mouiya^b, Abdelmjid Bouazizi^{e,f,g}, Younes Abouliatim^{a,c}, Houssine Sehaoui^b, Abdelaziz Benhammou^a, Said Mansouri^b, Hassan Hannache^d, Jones Alami^b, Abdelkrim Abourriche^{a,*}

^a Laboratory Materials, Processes, Environment and Quality, National School of Applied Sciences, Cadi Ayyad University (UCA), Route Sidi Bouzid BP 63, 46000, Safi, Morocco

^b Materials Science, Energy and Nanoengineering Department (MSN), Mohammed VI Polytechnic University (UM6P), Lot 660-Hay Moulay Rachid, 43150, Ben Guerir, Morocco

^c Laboratory of Process and Environmental Engineering (L.P.E.E), Higher School of Technology of Casablanca, Hassan II University, Route del Jadida, km 7, BP 8012, Oasis, Casablanca, Morocco

^d LIMAT-Thermostructural Materials and Polymers Team, Faculty of Science Ben M'sik, B.P. 7955, Casablanca, Morocco

^e Laboratory of Materials, Membranes and Nanotechnology, Faculty of Sciences, Moulay Ismail University, PB 11201, Zitoune, Meknes, Morocco

^f Department of Sciences, Ecole Normal Supérieure, Moulay Ismail University of Meknes, 50000, Morocco

^g Laboratory of Materials, Membranes and Environment, Faculty of Sciences and Technologies of Mohammedia, Hassan II University of Casablanca, Morocco

ARTICLE INFO

Keywords:

Moroccan red clay
Tea waste
Porous ceramic
Mechanical strength

ABSTRACT

The influence of the removal of carbonates on the ceramic properties made of Moroccan red clay as a main material and tea waste as pore-forming agent, has been investigated. ATD-TG, dilatometry, dimensional changes, weight loss, water absorption, open porosity, bulk density, flexural and indirect tensile strengths were assessed at different firing temperatures within the range of 900–1150 °C. SEM was used to evaluate the microstructures of the fired samples, while XRD was used to study the phase evolution. At varying firing temperatures, the materials which contains the carbonate (CC) exhibit greater weight loss, water absorption, and porosity compared to the materials without carbonate (NCC). On the other hand, NCC materials has greater mechanical strength than that CC materials. The microstructural analysis conducted through SEM revealed distinct changes in the fired samples when comparing observations at 1100 °C to those at 900 and 1000 °C. At 1100 °C, there was a noticeable increase in particle contacts and layered structures, which can be attributed to the presence of dehydroxylated clay minerals (illite and chlorite), quartz particles, and pores formed during firing. Subsequently, at 1150 °C/ 2 h, further alterations in the microstructures were observed due to a higher degree of vitrification in the fired samples. This resulted in material consolidation, interparticle and neck contacts, leading to the formation of vitrified bridges. Firing has resulted in the formation of closed and open pores of varying sizes, in the vitrified structures associated with anorthite, hematite, and quartz, a thin crystal precipitation of small particles was observed. This alteration in microstructure made it possible to conclude that the flexural and indirect tensile strength increased during firing, reaching its pinnacle at 1150 °C. As a result of the firing process, the ceramic supports underwent heightened sintering, leading to a gradual decline in open porosity. The present inquiry proved to be intriguing as it led to a deeper understanding of the utilization of Moroccan red clay as a ceramic's raw material.

Peer review under responsibility of King Saud University.

* Corresponding authors at: Laboratory of Materials, Processes, Environment and Quality, National Schools of Applied Sciences of Safi, B.P. 63 46000, University of Cadi Ayyad, Safi, Morocco.

E-mail addresses: yassine.rakcho@ced.uca.ma (Y. Rakcho), a.abourriche@uca.ma (A. Abourriche).

<https://doi.org/10.1016/j.arabjc.2023.105484>

Received 21 October 2023; Accepted 24 November 2023

Available online 25 November 2023

1878-5352/© 2023 The Authors. Published by Elsevier B.V. on behalf of King Saud University. This is an open access article under the CC BY-NC-ND license (<http://creativecommons.org/licenses/by-nc-nd/4.0/>).

1. Introduction

Ceramic membranes possess numerous advantages in comparison to organic membranes. These advantages encompass elevated permeability, commendable chemical and thermal stability, exceptional mechanical robustness, and prolonged durability (Rakcho et al., 2023). Nevertheless, a notable limitation of ceramic membranes resides in their elevated cost, which can be ascribed to the utilization of costly raw materials and the intricate sintering procedure. Commercial ceramic membranes are commonly manufactured using industrial oxides such as alumina, silica, titania, or their mixtures. These materials are known for their high cost and necessitate elevated sintering temperatures (Achiou et al., 2017; Karim et al., 2018). In recent times, there has been an increasing inclination towards the development of cost-effective ceramic membranes in order to boost their suitability for utilization in industrial applications. As a result, a considerable amount of research has been dedicated to the development of ceramic membranes utilizing cost-effective resources such as geomaterials and waste materials (Rakcho et al., 2023). A variety of geomaterials have been documented in the literature as being employed in the fabrication of cost-effective ceramic membranes. These include bentonite (Bouazizi et al., 2016), kaolin (Bouzerara et al., 2009), perlite (Majouli et al., 2012), pozzolan (Vizcayno et al., 2010), monolith (Arzani et al., 2018) and phosphate (Barrouk et al., 2015; Beqqour et al., 2019). It is worth noting that natural clays, in particular, have been extensively employed in the production of low-cost ceramic membranes, particularly for micro-filtration (MF) applications.

For instance, Elomari et al. (Elomari et al., 2017) conducted a study where they utilized clay and corn starch to create a MF membrane. They examined the impact of adding starch on various properties of the membrane, including permeability, porosity, shrinkage, and flexural strength. Another study by Belbi et al. (Belibi Belibi et al., 2015) focused on the production of a MF membrane using natural and local Cameroonian clay, which was then employed for the clarification of clay powder suspensions. Due to the presence of objectionable compounds like calcite, dolomite, and organic matter in natural clay, the use of clays in the preparation of ceramic membranes is currently restricted. Although the presence of carbonates and organic matter can increase the membrane's porosity and permeability, excessive quantities of these substances can result in larger pore sizes and cracks, especially when preparing thinner membrane layers that are more susceptible to thermal treatment. Consequently, the existence of impurities in natural clay can significantly compromise the properties of the membrane. To overcome these limitations, it is crucial to emphasize the purification of natural clay prior to its use in membrane preparation. Purification is strongly believed to be a key approach for developing membranes with superior performance.

The literature contains numerous studies that focus on employing commercially purified clays in the development of microfiltration (MF) or ultrafiltration (UF) membranes. For instance, montmorillonite clay has been utilized to enhance the permeability, thermal, and mechanical properties of polysulfone membranes (Rodrigues et al., 2019). A range of authors have reported on the use of bentonite clay to augment polymeric membranes for oilfield wastewater treatment applications. Ahmad and colleagues, for example, produced an affordable UF membrane by incorporating bentonite nano-clay into a polyvinyl chloride polymer, with the optimized membrane demonstrating effective oilfield water purification (Ahmad et al., 2018a). These researchers also explored the introduction of bentonite clay into a polyvinyl chloride UF membrane, with the aim of improving its hydrophilicity and antifouling capabilities (Ahmad et al., 2018b). In another study, a flat ceramic microfiltration membrane based on unpurified natural clay and Moroccan phosphate for desalination and industrial wastewater treatment, they found that the membrane demonstrated effective purification, average pore diameter of 2.5 μm and a satisfactory flexural strength of 17.5 MPa (Mouiya et al., 2018), however, these ceramic membranes are susceptible to

cracking when subjected to high pressure during filtration. The cracking can occur due to various reasons, including mechanical stress, thermal shock, and chemical reactions.

One of the main causes of ceramic membrane cracking during filtration is mechanical stress. The applied pressure can create stress in the membrane, leading to cracks and fractures. This stress can be caused by the high flow rate of the feed solution, which causes turbulence and pressure fluctuations in the membrane. Additionally, the presence of particles or impurities in the feed solution can cause abrasion and erosion of the membrane, leading to cracking. Chemical reactions can also lead to ceramic membrane cracking. The presence of aggressive chemicals, such as strong acids or bases, can react with the membrane material, leading to corrosion and weakening of the membrane structure. However, there are relatively few studies in the literature that focus on the application of purified natural clays in the development of ceramic membranes.

Given these considerations, the primary aim of this study is to examine the impact of alkaline earth carbonates removal from Moroccan red clay on the mechanical strength and porosity of ceramic supports. The presence of carbonates in the raw material used for manufacturing ceramic membranes can lead to reduced mechanical resistance, which limits their potential applications. To address this issue, this study will investigate the effect of carbonate removal on the mechanical properties and porosity of ceramic membranes, using red clay as the starting material. The research will involve characterization of the raw material and the resulting ceramic membranes, through various analytical techniques such as X-ray diffraction, scanning electron microscopy, mechanical testing and Archimedes principle test. The findings of this study could lead to the development of improved ceramic membranes with enhanced mechanical properties, and consequently, expanded applications in various industrial processes.

The second objective was to examine a wide spectrum of firing temperatures (900–1150 °C) to understand how variations in firing temperature impact the ceramic properties of these clays, such as mechanical strength (flexural and tensile strength), open porosity, bulk density, water absorption rate. This subject has not been investigated in previous studies of Moroccan red clay with carbonates (CC) and without carbonates (NCC).

2. Materials and methods

2.1. Raw materials

In this study, natural red clay sourced from the Safi region in Morocco, was employed as the primary material to develop ceramic microfiltration (MF) membranes. The clay underwent a series of processing steps, including grinding into a fine powder and sieving through a 50 μm mesh to ensure homogeneity. Additionally, tea waste of SINIA, a tea brand in Morocco, was obtained from the residual accumulation of tea waste at home. This waste was initially purified using distilled water to eliminate impurities and sugar residues, then subjected to a solar drying process for a duration exceeding five days. Subsequently, the dried waste was ground and sieved to achieve a uniform particle size distribution, with an estimated average particle size of 50 μm . The natural red clay and processed tea waste were combined in specified ratios to fabricate a ceramic support, incorporating 20 wt% of tea waste.

2.2. Removal of carbonates in the clay

To compare the influence of carbonates on the properties of ceramic supports, a portion of the raw clay was treated to eliminate these carbonate impurities, the fine powder was dispersed in water. An acetate buffer was used to keep the pH at 5.5, and an adequate volume of 0.1 M hydrochloric acid was added to initiate the reaction with carbonates. The mixture was gently agitated until no more carbon dioxide bubbles were observed, indicating complete decomposition of carbonates. The

resulting slurry was then rinsed with water and centrifuged until the supernatant was transparent and devoid of chlorides, as verified by the silver nitrate (AgNO_3) test. This clay, free from carbonate impurities, will be referred to as non-carbonated clay (NCC). On the other hand, the unprocessed clay, which includes carbonates, will be designated as Carbonated Clay (CC). Subsequently, ceramic supports are prepared using both types of clay, each integrated with a 20 % weight of tea waste that serves as a pore-forming agent, enabling a direct comparison of the influence of carbonate impurities on the characteristics of the resultant porous ceramic membranes.

2.3. Fabrication of flat porous ceramic

Cylindrical supports with dimensions of $20 \times 4 \text{ mm} \pm 0.5 \text{ mm}$ were fabricated utilizing powdered samples of CC and NCC. The powders were combined with tea waste at a weight percentage of approximately 20 % before to the pressing process. The cylindrical supports were acquired through the process of uniaxial dry pressing utilizing a laboratory press known as SPECAC, with an applied pressure of 95 MPa. The supports underwent a process of air-drying for a duration of 24 h, followed by oven-drying at a temperature of 110°C for a period of 24 h. The firing of these supports was conducted in an electric programmable furnace (Nabertherm) at a heating rate of $5^\circ\text{C}/\text{min}$. The firing temperatures ranged from 900 to 1150°C . A set of five samples, representative of each temperature, were subjected to a thermal treatment process in a furnace, commencing from an initial condition of room temperature. Following this heat treatment, the fired samples were gradually allowed to cool within the same furnace, until they reached room temperature. Subsequently, for conservation purposes, the samples were placed in an oven, where a consistent temperature of 110°C was maintained.

2.4. Thermal cycling

Heat treatment plays a critical role in the fabrication of ceramic materials. In this investigation, the heat treatment process was divided into four distinct stages:

- 1- Drying at 250°C for 4 h to eliminate residual moisture.
- 2- Thermally degrading TW organic matter at 450°C for 1 h.
- 3- Decomposing TW and dehydroxylating clay minerals at 750°C for 1.5 h.
- 4- Recrystallization annealing as the final processing step.

To prevent pellet cracking or deformation during heat treatment, a controlled temperature ramp rate of $5^\circ\text{C}/\text{min}$ was employed. The impact of sintering on the properties of porous ceramics was examined by employing four different final sintering temperatures: 900°C , 1000°C , 1100°C , and 1150°C .

2.5. Characterization techniques

The analysis of the crystalline phases in the sintered specimens was conducted employing X-ray diffraction (XRD) with a Bruker-AXS D8 powder diffractometer, which utilized $\text{Cu K}\alpha$ radiation ($\lambda\text{K}\alpha = 0.154186 \text{ nm}$). The content of carbonate ($\% \text{CaCO}_3$) was determined by Bernard calcimeter. To assess the evolution of open porosity and bulk density in the sintered specimens, the Archimedes principle test was employed, using water as the immersion fluid. The microstructure of the sintered specimens was visualized via scanning electron microscopy (SEM) using a Hitachi SC 2500 instrument, with an accelerating voltage range of 10 to 30 kV. The analysis of the alterations in the flat compact geometry resulting from heating was conducted utilizing a horizontal dilatometer, namely the Linseis L75PT model.

Differential thermal analysis (DTA) and thermogravimetric (TG) analysis were conducted using a Setaram SETSYS 24 instrument, with $\alpha\text{-Al}_2\text{O}_3$ employed as the reference material. The samples under investigation were subjected to heating up to 1100°C , with a controlled heating rate of $10^\circ\text{C}/\text{min}$.

The mechanical properties of the sintered specimens were examined using Brazilian tests and three-point flexural tests, conducted on an Ametek Lloyd Instruments testing system. Load-displacement curves for mechanical strength measurements were obtained at a loading rate of 0.1 mm min^{-1} . The test cylinders featured dimensions of 19.8 mm in diameter and 4.5 mm in height. Indirect tensile strengths (σ_T) were calculated according to Eq.(1), and three-point flexural strengths (σ_F) were determined using Eq.(2).

$$\sigma_T = \frac{F_T}{S} = \frac{2F_T}{\pi Dh} \quad (1)$$

$$\sigma_F = \frac{3 F_F L}{2 w t^2} \quad (2)$$

The dimensions of the rectangular specimens are represented by w (width) and t (thickness), both measured in mm. Similarly, the cylindrical specimens' dimensions are denoted by D (diameter) and h (height), also in mm. The maximum loads experienced at the point of fracture are indicated by FF and FT , both measured in Newtons (N). The distance between the supports (L) has a measurement of 31 mm .

3. Results and discussion

3.1. Characterization of raw materials

3.1.1. Chemical composition

The comprehensive chemical profile of the unprocessed clay is detailed in Table 1. This profile predominantly encompasses silicon dioxide (SiO_2), aluminum oxide (Al_2O_3), calcium oxide (CaO), iron(III) oxide (Fe_2O_3), and potassium oxide (K_2O), while the presence of magnesium oxide (MgO), sodium oxide (Na_2O), titanium dioxide (TiO_2), and phosphorus pentoxide (P_2O_5) is comparatively less. The highest concentration of oxides, namely SiO_2 and Al_2O_3 , are majorly linked with the composition of quartz and clay minerals, including illite, mullite, and kaolinite, which are ubiquitously found in clay. Furthermore, an elevated $\text{SiO}_2/\text{Al}_2\text{O}_3$ ratio points towards a considerable presence of quartz and/or amorphous silica (Achiou et al., 2016).

The quantification of calcite content was carried out employing the Bernard calcimeter method, which divulged that raw clay comprises 11 wt% of calcium carbonates (CaCO_3). It can be inferred that a significant proportion of the detected CaO content via X-ray fluorescence (XRF) analysis is embodied as dolomite and calcite. The recorded loss of ignition at a temperature of 1100°C is attributable to the breakdown of carbonates, burning of organic substances, and removal of hydroxyl groups from clay minerals (Teklay et al., 2014).

3.1.2. FTIR analysis

The Fourier-transform Infrared (FTIR) analysis results for raw clays (CC), as depicted in Fig. 1, reveal distinctive bands at 470 and 535 cm^{-1} . These bands are associated with the stretching vibrations of Si-O-Mg, and Si-O-Al (Miyah et al., 2017). The Si-O stretching vibration exhibits a pronounced and well-defined band at 1036 cm^{-1} . Concurrently, $\text{Al}_2\text{-OH}$ stretching and bending bonds, intrinsic to phyllosilicates, give rise to a band at 3624 cm^{-1} (Mudrinić et al., 2015). The FTIR band at 3436 cm^{-1} is likely attributable to $-\text{OH}$ stretching mode. A bending vibration band indicative of water hydration is also visible around 1640 cm^{-1} . An absorption band noted at 1425 cm^{-1} is characteristic of carbonates, and the bands at 690 and 778 cm^{-1} serve as markers for quartz (Thuc et al., 2010). Contrastingly, the FTIR spectra for purified Clay (NCC), presented in Fig. 1, demonstrate the notable absence of the characteristic band at 1425 cm^{-1} . This absence strongly suggests that purified clays are devoid of carbonates, a finding which aligns seamlessly with prior X-ray Diffraction (XRD) characterizations and Bernard calcimetry results. This concordance provides a positive indication of the purification's efficacy.

On the other hand, the FTIR spectrum of tea waste is illustrated in

Table 1
Chemical composition of raw red clay (wt%).

	SiO ₂	Al ₂ O ₃	Fe ₂ O ₃	CaO	K ₂ O	P ₂ O ₅	TiO ₂	Na ₂ O	MgO	SO ₃
Wt. %	56.203	15.109	9.695	6.669	4.677	1.455	1.416	0.383	1.215	0.279

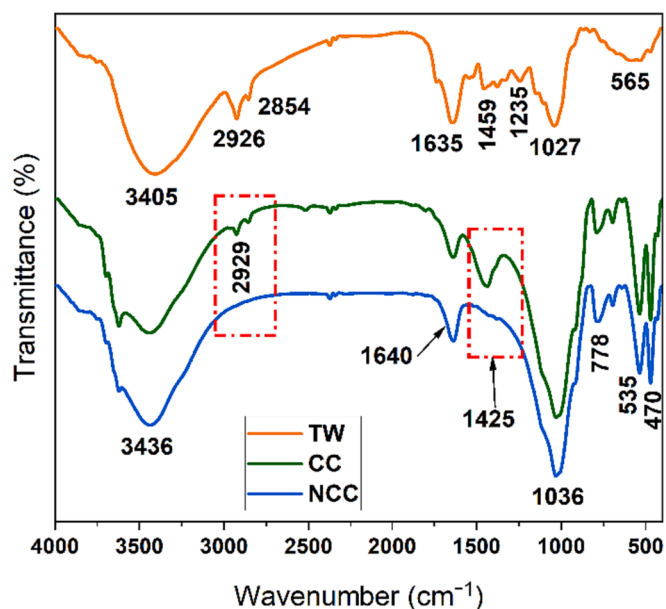


Fig. 1. FTIR spectrum of calcareous clay (CC), non-calcareous clay (NCC) and tea waste (TW).

Fig. 1. An extensive absorption band ranging from 3010 to 3705 cm^{-1} , which is often associated with the O–H and N–H stretching vibrations seen in polyphenols, as highlighted in previous studies (Loo et al., 2012; Senthilkumar and Sivakumar, 2014). Saif et al. (Saif et al., 2016) suggested that the substantial absorption band detected at 3310 cm^{-1} , can be linked to the presence of hydroxyl functional groups (OH), which are common in alcohols and phenolic compounds.

Moreover, a prominent band at 1636 cm^{-1} is recognized, typically corresponding to the stretching vibrations of C = C bonds in aromatic rings and C = O bonds in polyphenolic compounds (Dubey et al., 2017; Senthilkumar and Sivakumar, 2014). Vibrational bands for the C–H stretch in alkane and the O–H stretch in carboxylic acid are apparent at 2926 cm^{-1} and 2854 cm^{-1} respectively (Dubey et al., 2017). A notable band at 1027 cm^{-1} is assigned to the C–O stretching in amino acids (Dubey et al., 2017; Senthilkumar and Sivakumar, 2014).

J.Cai et al. (Cai et al., 2015) identified similar FTIR bands across multiple tea types, including oolong, green, and black tea. Previous research has mapped the infrared bands of polyphenols in tea at 3387 cm^{-1} , 1635 cm^{-1} , and 1027 cm^{-1} ; these are correlated with N–H/O–H, C = C, and C–O–C stretches, respectively (Dubey et al., 2017; Senthilkumar and Sivakumar, 2014; Weng et al., 2013). The FTIR spectrum thus reveals that the dominant functional groups in tea residue include carboxylic acid, polyphenols, and amino acids.

3.1.3. XRD analysis

The X-Ray Diffraction (XRD) patterns for both the calcareous clay (CC) and the non-calcareous clay (NCC) are depicted in Fig. 2. The reflection spectra from the calcareous clay (CC) are attributed to the prevalent phases of quartz, illite, calcite, and dolomite. However, the XRD patterns of the purified clay (NCC) show a different composition. The main components of this purified clay include quartz, kaolinite, illite, and chlorite, indicating that these are the primary clay minerals present. Notably, there is an absence of any detectable peaks for calcite

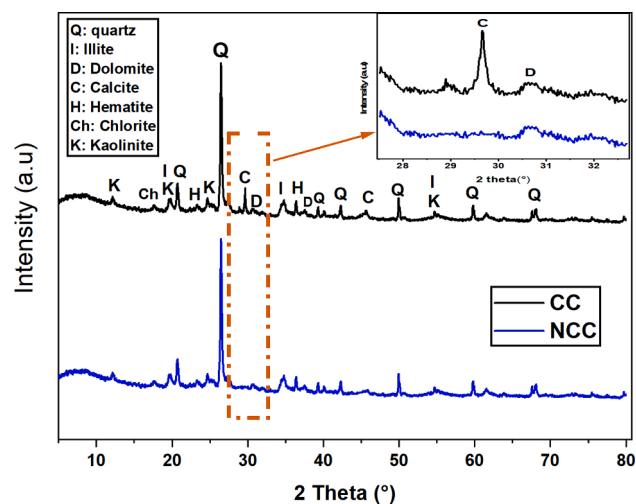


Fig. 2. DRX of calcareous clay (CC) and non-calcareous clay (NCC).

and dolomite, implying that these impurities have been fully eliminated. Thus, according to the XRD findings, it can be inferred that the purified clay exhibits an enrichment of clay minerals and a significant reduction in impurities such as calcite and dolomite.

3.1.4. Thermal analysis

The organic phases (Tea waste) must be eliminated entirely when sintering the green ceramic support in order to generate the necessary porosity ceramics without causing any flaws. ATD/TG analysis was performed to determine a heating schedule, and the outcome is depicted in Fig. 3. It presents the analysis of a mixture comprising 20 wt% of tea waste and 80 wt% of raw clay (CC). With escalating temperatures, a progressive yet uneven weight reduction is noticed, totaling a weight loss of 35.32 wt%. At temperatures less than 100 °C, there's an initial weight reduction of 5.31 wt%, ascribed to the endothermic evaporation of unbound water. A subsequent 10.41 wt% weight loss in the temperature range of 100–320 °C may be due to the elimination of adsorbed water and the expulsion of volatile organic compounds. In the temperature bracket of 320–560 °C, an additional weight loss of 14.20 wt% is identified, which could be traced to the disintegration of remaining organic compounds with firmly bonded carbonyl and hydroxyl groups. This is also attributed to the dehydroxylation of clay minerals such as illite and kaolinite, and the transformation of α -quartz into β -quartz (Mouiya et al., 2022; Vizcayno et al., 2010).

Around 705 °C, an endothermic peak is recorded alongside a 5.40 wt % weight reduction, suggesting the thermal decomposition of mineral carbonates. Post 900 °C, no considerable decrease in weight is discernible. The thermal evaluation advocates that the sintering of ceramic membranes should ideally occur at temperatures exceeding 900 °C.

3.1.5. Dilatometric analysis

Due to thermal agitation, heating a substance increases its internal energy. The expansion coefficient is a proportionality factor that correlates with the increase in average interatomic distances with temperature. Measuring a material's expansion typically only allows us to characterize its linear expansion. The coefficient of linear expansion (α) may be calculated at each temperature using the relationship (3), where L is the length of the specimen.

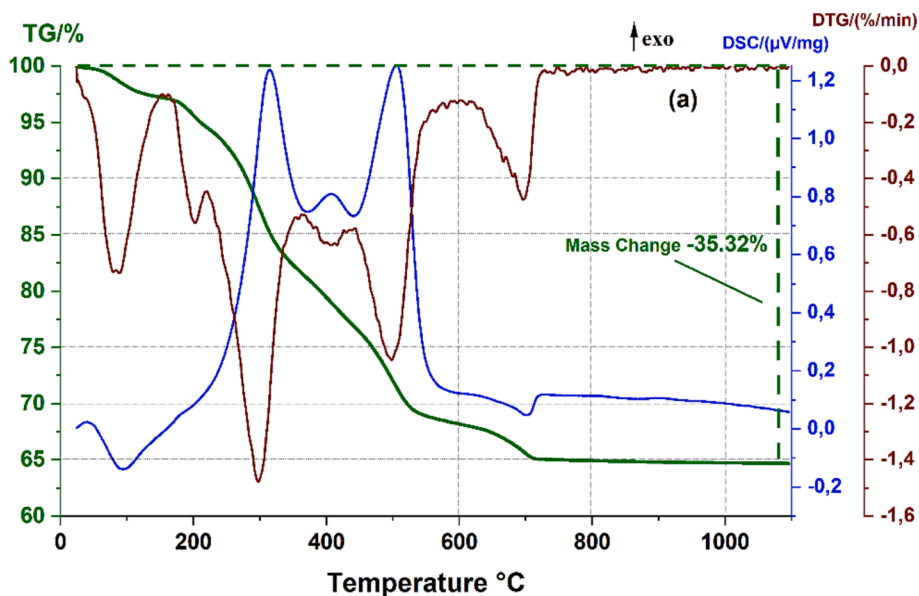
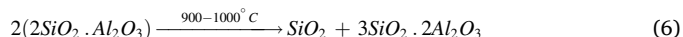
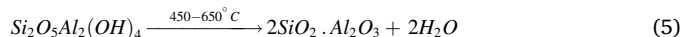
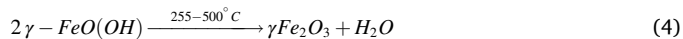


Fig. 3. ATD/TG of raw red clay (CC) mixed with 20 wt% of tea waste.

$$\alpha = \frac{\Delta L}{L_0 \times \Delta t} \quad (3)$$

The thermal expansion behaviour depicted in Fig. 4 exhibits a pronounced curve between heating and cooling. This graph depicts three noteworthy shifts in behavior as the temperature increases to 1100 °C. The initial expansion occurring between 155 and 230 °C can be attributed to the release of loosely bound and accumulated water from the interlayer regions of the specimen. The significant secondary expansion ranging from 330 to 588 °C aligns with the breakdown of the organic components present in TW, and around 573 °C, a slight expansion singularity highlights the α to β transition of quartz, which is the so-called quartz dilatometric anomaly (Mouiya et al., 2022). In addition, at this point clay minerals lose structural water, such as lepidocrocite (FeO (OH), which, following dehydration, produces hematite (Fe₂O₃), (Eq. (4)) (Morris et al., 1998) and kaolinite (Al₂Si₂O₅(OH)₄) is transformed to metakaolin through the so-called kaolinite network collapse, in which the Si–O links stay intact but the Al–O network is reorganized (Eq. (5)) (Kakali et al., 2001). The substantial shrinkage between 855 and 1100 °C was attributed to the presence of Si site rearrangement processes that produced cristobalite (SiO₂) and mullite (3SiO₂·2Al₂O₃) (Eq. (6)) (Faieta-Boada and McCollm, 1993). The preceding assignments were

validated by XRD (Fig. 5). The coefficient thermal expansion (CTE) of the green compact between 230 and 330 °C was calculated to be $5.75 \times 10^{-6} \text{ }^\circ\text{C}^{-1}$, and $7.14 \times 10^{-6} \text{ }^\circ\text{C}^{-1}$ between 588 and 720 °C assuming linear expansion.



3.2. XRD analysis of ceramic supports

In Fig. 5, the DRX of the ceramic supports after being fired at temperatures of 900, 1000, 1100, and 1150 °C for 2 h are presented. The analysis reveals significant changes in the mineral composition of the clay sample. The original minerals found in the clay, such as calcite, illite, kaolinite, and chlorite, are no longer detectable after the heat treatment. Instead, new phases have emerged.

At a temperature of 900 °C, the presence of kaolinite (Al₂Si₂O₅(OH)₄) becomes undetectable as it undergoes a transformation

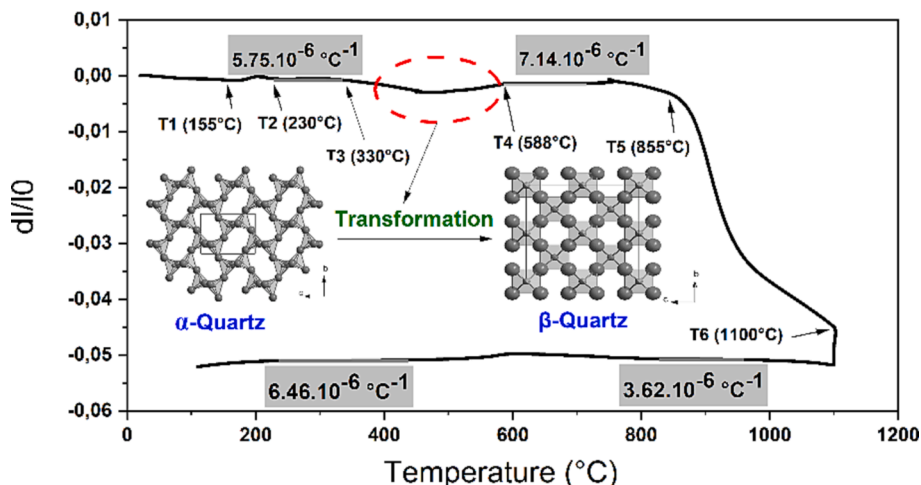


Fig. 4. Thermal expansion behavior of raw red clay containing 20 wt% of tea waste during sintering up to 1100 °C.

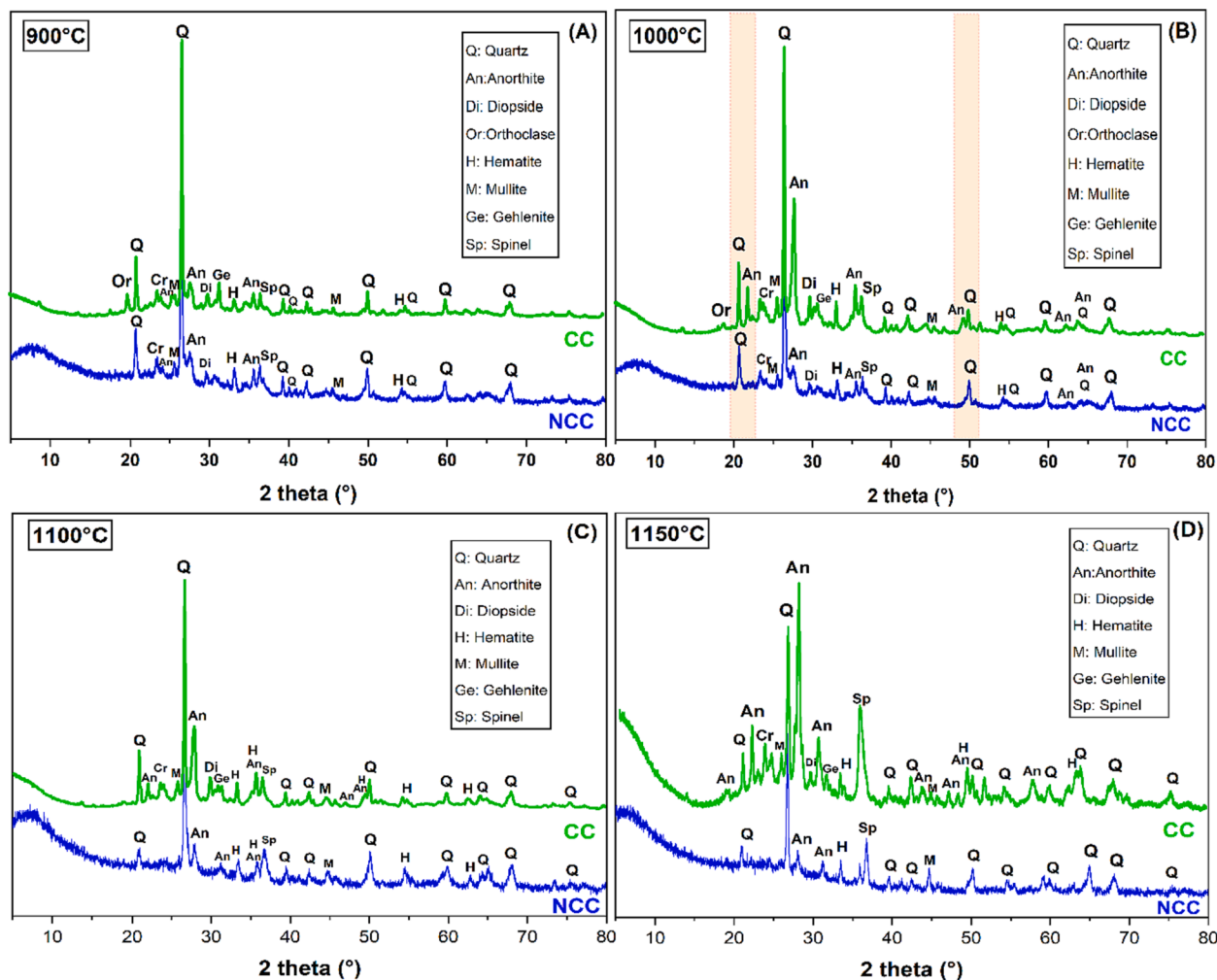


Fig. 5. XRD diagrams of CC and NCC samples fired at (a) 900 °C, (b) 1000 °C, (c) 1100 °C and 1150 °C.

into metakaolinite. This transformation occurs through the removal of hydroxyl groups from the silicate component at temperatures exceeding 450 °C (El Ouahabi et al., 2015). The mineral anorthite ($\text{CaAl}_2\text{Si}_2\text{O}_8$) emerges as a newly formed compound at 900 °C, with its highest concentration observed at 1150 °C. This creation of anorthite is likely a consequence of complex, step-by-step solid-state reactions between the clay matrix and carbonate compounds (El Ouahabi et al., 2015; Manni et al., 2019).

Gehlenite ($\text{Ca}_2\text{Al}_2\text{SiO}_7$) and spinel (MgAl_2O_4) are initially identified at a temperature of 900 °C, and their quantities become more discernible as the temperature rises to 1100 °C. The genesis of gehlenite occurs through the interaction of calcium oxide (CaO) from calcite with metakaolinite (Manni et al., 2019). In contrast, spinel is generated via a reaction involving magnesia (MgO) and alumina (Al_2O_3). The source of MgO is derived from the dehydroxylation process of chlorite and dolomite minerals, while alumina (Al_2O_3) is a product of the disintegration of clay minerals and K-feldspar (Manni et al., 2019).

The peaks corresponding to orthoclase are detected at a temperature of 900 °C, however, they are no longer present at a temperature of 1000 °C. This disappearance is due to their contribution to the creation of the mullite phase (Cultrone et al., 2001). Quartz (SiO_2) is the only primary mineral that can withstand temperatures as high as 1150 °C. The presence of quartz peaks is observed across all firing temperatures; however, their intensity decreases at higher temperatures due to dissolution or transformation into smaller quantities of cristobalite (El Ouahabi et al., 2015).

Mullite is present in minor amounts at all tested temperatures

(900–1150 °C), which may be attributable to the presence of adequate illite content. After illite is destroyed by hydroxylation, it reacts with quartz, resulting in the transformation of quartz into mullite (Manni et al., 2019). Diopside ($\text{CaMgSi}_2\text{O}_6$) is presumably produced by the high-temperature reaction of CaO, MgO, and SiO_2 . CaO may have originated from calcite and dolomite, whereas MgO is likely derived from chlorite and dolomite. The formation of diopside is predominantly characterized by a sharp decrease in the proportion of quartz (El Ouahabi et al., 2015).

Conversely, in the non-carbonate clay (NCC), orthoclase, diopside, and mullite were not identified, an outcome attributed to the extraction of carbonate from the raw clay utilized for NCC. In scenarios where carbonate persists in the raw clay, a chemical reaction occurs between calcium oxide (CaO) and silicon (Si), yielding calcium silicates like gehlenite and diopside, which are notably absent in the decarbonated clay (NCC).

Moreover, anorthite was observed in lesser amounts in non-carbonate clay (NCC) compared to its significant presence in carbonate clay (CC) at 1150 °C. The quantity of quartz, however, was noted to decline at this peak firing temperature. While anorthite, hematite, and quartz remained detectable across the entire spectrum of temperatures.

3.3. Ceramic properties

3.3.1. Weight loss, size and color variation caused by sintering at different temperatures

Table 2 provides a comprehensive analysis of weight losses and dimensional variations (diameter and thicknesses) in pressed ceramic

Table 2

Weight losses and changes in dimensions (diameter and thickness) of ceramic supports derived from powdered samples CC and NCC as firing temperatures increased.

Sample	Firing temperature (°C)	Weight loss (wt. %)	Variation in thickness (%)	Variation in diameter (%)
CC	900	19.3 ± 0.45	0.48 ± 0.04	1.10 ± 0.05
	1000	21.10 ± 0.21	0.97 ± 0.06	2.30 ± 0.08
	1100	25.17 ± 0.54	2.88 ± 0.05	6.90 ± 0.31
	1150	33.73 ± 0.18	4.69 ± 0.14	9.41 ± 0.28
NCC	900	17.88 ± 0.27	0.42 ± 0.07	1.04 ± 0.06
	1000	20.92 ± 0.49	0.85 ± 0.08	2.23 ± 0.09
	1100	24.93 ± 0.09	2.74 ± 0.12	6.79 ± 0.15
	1150	31.03 ± 0.22	4.57 ± 0.17	9.20 ± 0.24

supports derived from CC and NCC samples, which were subjected to increasing firing temperatures ranging from 900 °C to 1150 °C. The results demonstrate significant changes in weight losses for the CC sample as the firing temperature escalates. The experimental data showcases a range starting from 19.3 ± 0.45 wt% at 900 °C / 2 h and reaching a maximum value of 33.73 ± 0.18 wt% at 1150 °C / 2h. Comparatively, the weight losses observed in the NCC sample are slightly lower than those of the CC sample. The weight loss values exhibit a similar trend, with a minimum of 17.88 ± 0.27 wt% at 900 °C / 2h and a maximum of 31.03 ± 0.22 wt% at 1150 °C / 2 h. As shown in Fig. 3 (ATD-TG), the observed weight variations in the fired ceramic supports can be predominantly ascribed to the removal of organic substances, dehydroxylation of clay minerals such as chlorite and illite, and decarbonation of calcite within the CC sample.

Fig. 6 displays a collection of chosen test specimens obtained from the samples that underwent firing from 900 to 1150 °C for a duration of 2 h. The firing process induces noticeable changes in dimensions, accompanied by a color transition from red to a deep shade of dark red. This color alteration can be attributed to the presence of Fe₂O₃ in the samples, as indicated by the chemical analysis presented in Table 1. The color transformation in ceramics is a multifaceted process influenced by various physico-chemical and mineralogical factors (Raigón-Pichardo et al., 1996). In a recent study by Harrati et al. (Harrati et al., 2022), Clayey samples including kaolinite, illite, quartz, calcite and chlorite were studied. The authors suggested that a higher content of Fe₂O₃ (>3 wt%), similar to the conditions in our study, could result in a reddish coloration after firing. This observation aligns with the visual examination of the ceramic supports derived from CC and NCC samples, as depicted in Fig. 6.

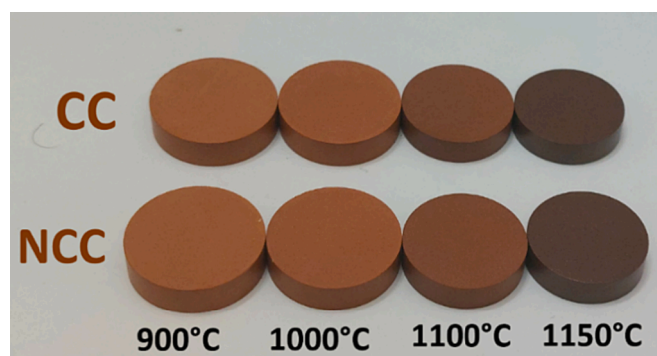


Fig. 6. Image depicting the ceramic supports manufactured from the samples CC and NCC at various temperatures.

3.3.2. Bulk density, open porosity and water absorption

Open porosity and bulk density analyses, is shown in Fig. 7, were conducted on two supports ceramic samples: one incorporated carbonate (CC) while the other (NCC) was devoid of this component. A series of tests were conducted at varying temperatures, unveiling intriguing correlations and dependencies on the presence of carbonates.

At 900 °C, the density of the carbonate-inclusive sample (CC) was 1.39 g/cm³, contrasted by a slightly higher 1.47 g/cm³ in the carbonate-free sample (NCC). Concurrently, the open porosity in the carbonate-bearing ceramic was 48.51 %, compared to 41.82 % in the sample devoid of carbonates. This disparity points to the potential role of carbonates in fostering greater porosity, possibly by contributing to the formation of pores during the thermal treatment.

At 1000 °C and 1100 °C, the presence of carbonates corresponded with a lower density and a higher porosity compared to the carbonate-free counterpart. At 1000 °C, the carbonate-inclusive sample showed a density of 1.48 g/cm³ and a porosity of 43.3 %. In contrast, the sample without carbonates displayed a density of 1.53 g/cm³ and a porosity of 38.44 %. Similarly, at 1100 °C, the densities were 1.55 g/cm³ (carbonate-inclusive-CC) and 1.59 g/cm³ (carbonate-free-NCC), with porosities of 39.35 % and 33.15 % respectively. These trends suggest that carbonate presence may be influencing the ceramic microstructure, thereby affecting the porosity and density.

However, at 1150 °C, a dramatic divergence was observed. Both samples experienced a significant increase in density (carbonate-inclusive: 2.01 g/cm³, carbonate-free: 2.09 g/cm³) and a corresponding decrease in open porosity (carbonate-inclusive-CC: 18.87 %, carbonate-free-NCC: 17.11 %). It suggests a substantial structural transition potentially due to a phase transformation, sintering progressively at higher temperatures results in the production of a denser ceramic body (see SEM, in Fig. 9-D). This densification is achieved through the creation of a glassy phase that effectively fills the material's pores. According to Semiz's study (Semiz, 2017), it is probable that the rise in bulk density during firing is linked to the development of a prominent glassy phase. This leads to an increase in the formation of a liquid phase and consequently a reduction in the material's porosity. The carbonate-inclusive sample still maintained lower density and higher porosity than the carbonate-free one.

These findings underscore the significant impact of carbonates on the density and open porosity of supports ceramic. The presence of carbonates seems to enhance the porosity and reduce the bulk density at lower temperatures, while even at high temperatures where densification occurs, carbonates appear to limit this densification to an extent. The exact mechanisms by which carbonates influence these properties would be a compelling subject for further exploration.

It should be noted that the influence of carbonate content on the pore size in ceramics, and consequently on their potential as filtration media, presents a complex interplay of benefits and potential drawbacks that need to be evaluated critically. The presence of carbonates has been observed to increase open porosity, which in turn increases pore size. While at first glance this might seem advantageous for filtration applications, as larger pores would allow for higher flow rates, this effect should not be considered in isolation.

The size and distribution of pores in a filter medium directly affect its performance. Larger pores might indeed facilitate greater flow rates, reducing the pressure needed for filtration and increasing the filter's overall capacity. However, they could also compromise the filter's ability to capture and retain small particles, thus reducing the filter's efficiency in terms of particle removal. If the aim is to filter out microscopic contaminants, an increase in pore diameter induced by carbonates might not be beneficial, but rather detrimental to the performance of the filter.

Furthermore, increased porosity and larger pores could lead to decreased mechanical strength, as larger pores can act as stress concentrators, leading to premature failure under mechanical or hydraulic pressure. This is a crucial factor for ceramic filters, which often operate

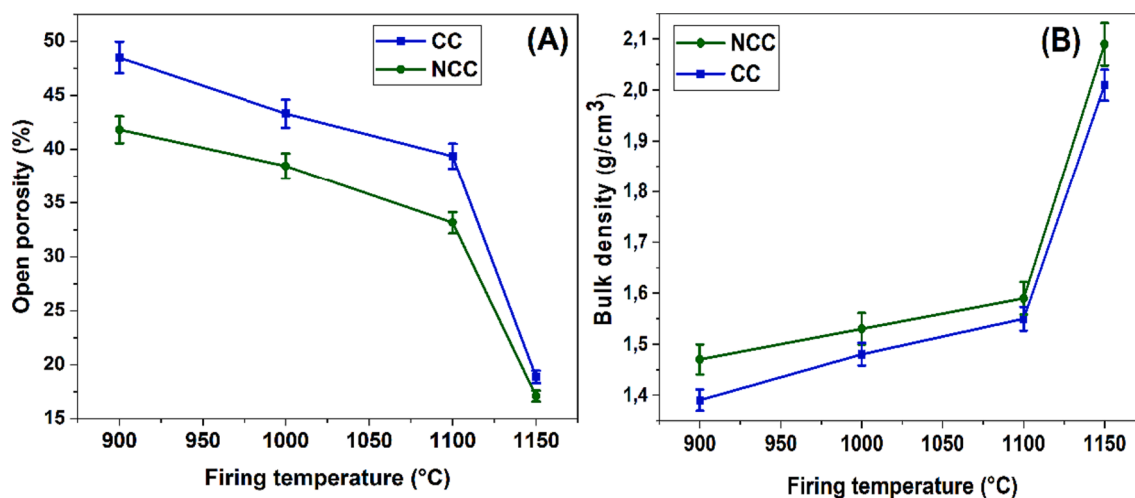


Fig. 7. Open porosity (A) and bulk density (B) results for CC and NCC fired samples.

under significant pressure differentials.

In addition, the water absorption capacity is a useful metric for analyzing the densification process and the quality of ceramic supports, which is determined by the volume of open pores that can absorb water in the fired specimens. The water absorption capacities for CC and NCC samples in Fig. 8 show that the former's capacity declines from 33.2 ± 0.51 % at 900 °C for 2 h to 23.6 ± 0.48 % at 1100 °C for the same duration. It further drops sharply to 12.9 ± 0.40 % at 1150 °C for 2 h. The NCC samples demonstrate a similar trend. A variation of approximately 20 % in the water absorption capacity is recorded for both sample types when heated from 900 to 1150 °C/2h. In a study conducted by Semiz et al. (Semiz, 2017), the water absorption capacity of illite-smectite-kaolinitic clays varied from 20 % at 700 °C to 2 % at 1200 °C. They posited that this shift is likely associated with the emergence of a glassy phase.

Furthermore, the results illustrated in Fig. 8 demonstrate that the presence of carbonates in CC samples leads to an increase in the water absorption of ceramic supports, independently of firing temperature. This enhancement is to be expected, as the carbonates present in the raw clay (CC) decompose into CO_2 as the firing process proceeds, the open porosity of the ceramic support samples increases (Arslan et al., 2021; Ngayakamo et al., 2020; Njeumen Nkayem et al., 2016).

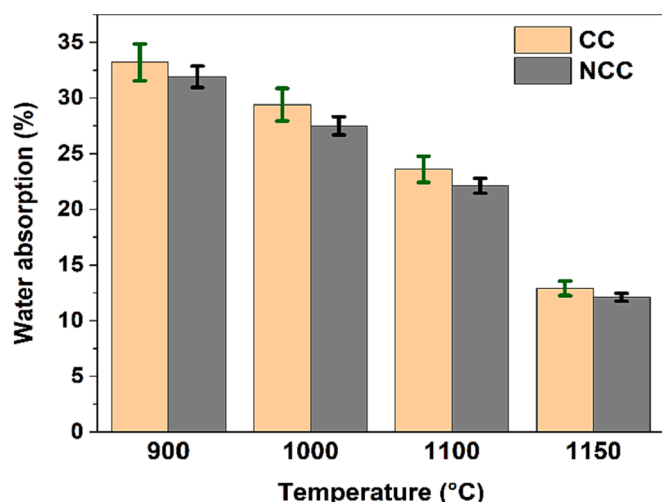


Fig. 8. Water absorption results for CC and NCC fired samples.

3.3.3. SEM microstructural analysis of fired samples

The SEM analysis focused on investigating the changes in microstructure of NCC samples after firing. Fractured surfaces were examined to observe these microstructural variations. In this section, we provide specific SEM micrographs of NCC samples that have been subjected to firing within the temperature range of 900 to 1150 °C. The SEM evolution of the NCC samples is illustrated in Fig. 9. Initially, up to a temperature of 900 °C/ 2 h, the microstructure of the material remains unaltered. This can be attributed to the fact that the pressed and fired samples still retain the layered structure of clay minerals (particularly illite and chlorite), which remains discernible. However, the illite undergoes dehydroxylation, while the chlorite decomposes. This observation aligns with previous studies and SEM investigations on the thermal treatment of clay minerals (Sanchez-Soto and Perez-Rodriguez, 1989). Moreover, the micrographs reveal the presence of a porous structure, with an open porosity of 41.82 % (as depicted in Fig. 7). This porosity is a consequence of the dehydroxylation process occurring in the clay minerals. Additionally, the presence of compact crystalline formations of varying sizes in the fired samples can be linked to quartz grains that are integrated within the matrix.

When subjected to a temperature of 1000 °C for a duration of 2 h, the early phases of the vitrification process become. This process manifests in the formation of minute pores, along with the potential merging of the layered structures, such as dehydroxylated illite and decomposed chlorite. Despite this coalescence, layered structures remain identifiable on the fracture surface. The sample's open porosity is approximately 38.44 %, lower than the porosity observed in the sample fired at 900 °C/2h.

At a temperature of 1100 °C for a duration of 2 h, a significant change occurs in the SEM of the fracture surface of the fired samples. This change is characterized by a reduction in the size of pores, indicating a diminution in porosity. The open porosity of the samples shows a slight decrease (33.15 %, Fig. 7) compared to samples fired at lower temperatures of 900 °C/ 2 h and 1000 °C/2h (as shown in Fig. 7). Moreover, the matrix contains small crystalline particles, specifically associated with quartz.

At a temperature of 1150 °C maintained for 2 h, the degree of vitrification in the fired sample is higher and more widespread, resulting in a distinct microstructure compared to earlier observations (as seen in Fig. 9, the SEM of samples fired from 900 to 1100 °C for 2 h). Indeed, the existence of alkaline and alkaline-earth oxides plays a significant role in developing the vitreous phase, which becomes liquid at high temperatures and is discernible in the SEM of the samples generated through firing. SEM reveals a more intricate microstructure. Additionally, there's a decrease in open porosity to around 17.11 % (as depicted in Fig. 7) and an increase in the bulk density (~ 2.09 g/cm³, as shown in Fig. 7).

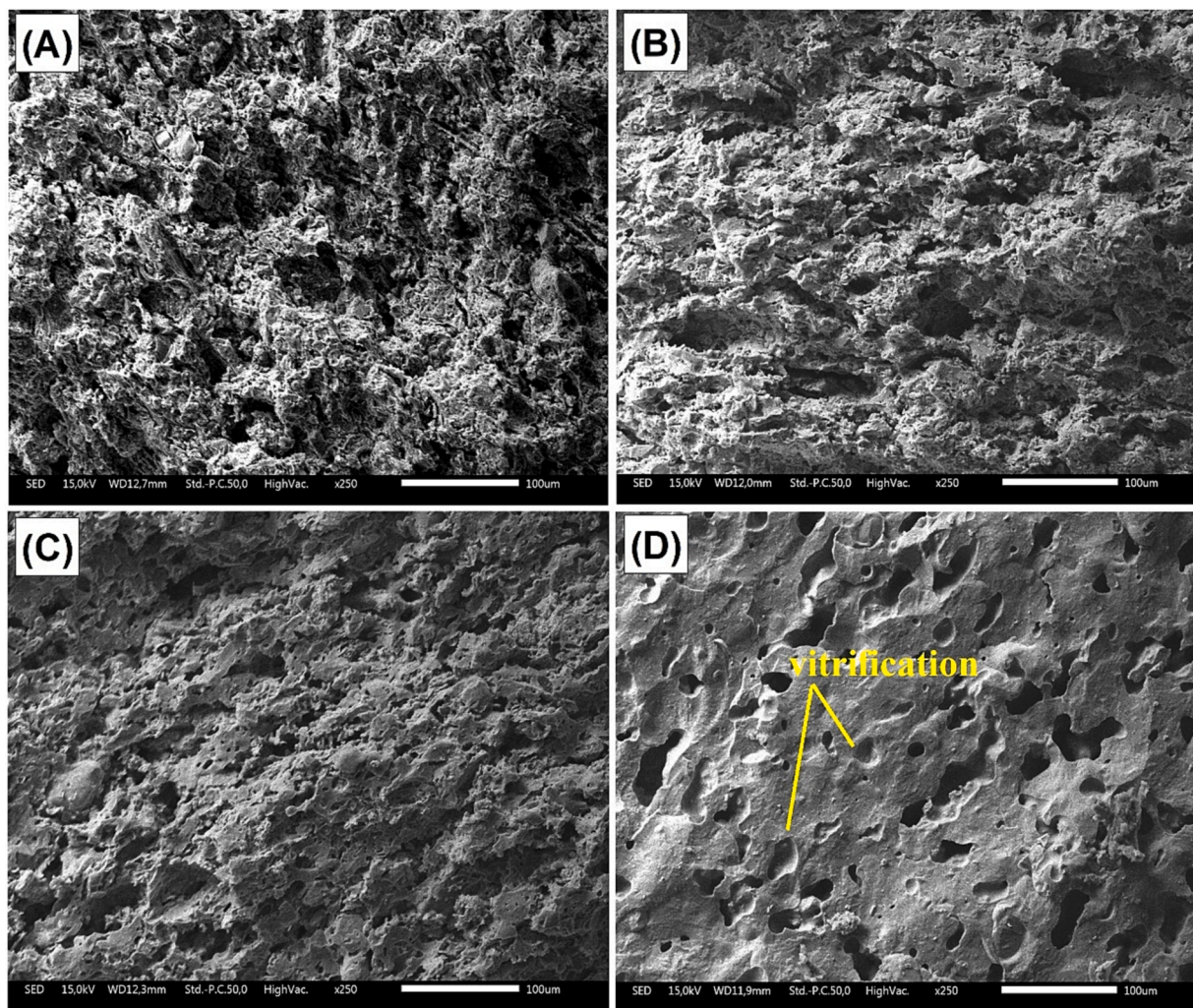


Fig. 9. SEM micrographs of sample NCC fired at 900 °C (A), 1000 °C (B), 1100 °C (C) and 1150 °C (D).

3.3.4. Mechanical strength

3.3.4.1. Flexural and indirect tensile strength. The outcomes pertaining to the flexural and tensile strength of both fired samples, namely CC and NCC, are illustrated in Figs. 10 and 11 correspondingly. In the case of the CC sample, the highest flexural strength value recorded is 42.47 ± 3.24 MPa, achieved through firing at 1150 °C for 2 h. Similarly, for the NCC sample, a similar trend is observed, with the flexural strength reaching 44.84 ± 2.86 MPa under the same firing conditions of 1150 °C for 2 h. Broadly speaking, the results indicate that subjecting the samples to firing temperatures higher than 900 °C for 2 h leads to an elevation in their flexural strength. This enhancement is attributed to the gradual development of a glassy phase, effectively filling the minute pores within the samples. This finding aligns with the SEM (Fig. 9-D), which exhibits a substantial, compact surface area characterized by the complete absence of tiny pores. The presence of crystalline solid phases (diopside and anorthite) contributed to the enhancement of flexural strength. In the case of samples sintered at 900 and 1000 °C (depicted in Fig. 10-B), a linear progression with heightened elasticity prior to failure was observed, attributed to their exceptional elasticity. However, when examining the tensile load–displacement curves of the supports sintered at 1150 °C, two distinct behaviors emerged. Initially, the material exhibited limited plasticity, succeeded by a substantial increase leading to sudden failure. This crucial observation underscores that the elasticity of the red clay material diminishes beyond 1150 °C during high-temperature sintering.

On the other hand, the results reveal that the flexural strength values increase significantly in the decarbonized samples (NCC) at all sintering temperatures. This increase can be explained by a slight reduction in open pores, as shown in Fig. 7, due to the absence of carbonates, which leads to a considerable increase in flexural strength.

Fig. 10 illustrates the plot of the indirect tensile strength values for the sample CC, the indirect tensile strength is 5.03 ± 1.1 MPa at a firing temperature of 900 °C for 2 h, which represents the minimum value. As the firing temperature increases, the indirect tensile strength values also increase, reaching a maximum of 17.66 ± 2.75 MPa at 1150 °C for 2 h. At this maximum point, the water absorption capacity is 12.9 ± 0.64 % (Fig. 8) and the open porosity is 18.87 ± 0.56 % (Fig. 7). The most significant change in indirect tensile strength occurs starting from 1100 °C for 2 h and continues at higher firing temperatures.

For the sample NCC in Fig. 11, the values of indirect tensile strength increase almost linearly, starting from 6.65 MPa at a firing temperature of 900 °C for 2 h and reaching similar values at 900–1100 °C for 2 h. Beyond 1100 °C for 2 h, the indirect tensile strength of the sample exhibits a swift growth, peaking at 19.52 MPa at a temperature of 1150 °C, over a duration of 2 h. At this pinnacle, the water absorption capacity stands at 12.1 ± 0.36 % (as shown in Fig. 8), while the open porosity reaches 17.11 ± 0.51 % (as depicted in Fig. 7). Nevertheless, the maximum value recorded for the samples NCC on the same firing temperature (19.52 ± 0.81 MPa) better than that achieved by the samples CC (17.66 ± 0.53 MPa). Hence, the decline in open porosity (as illustrated in Fig. 7) and the reduction in water absorption capacity (as

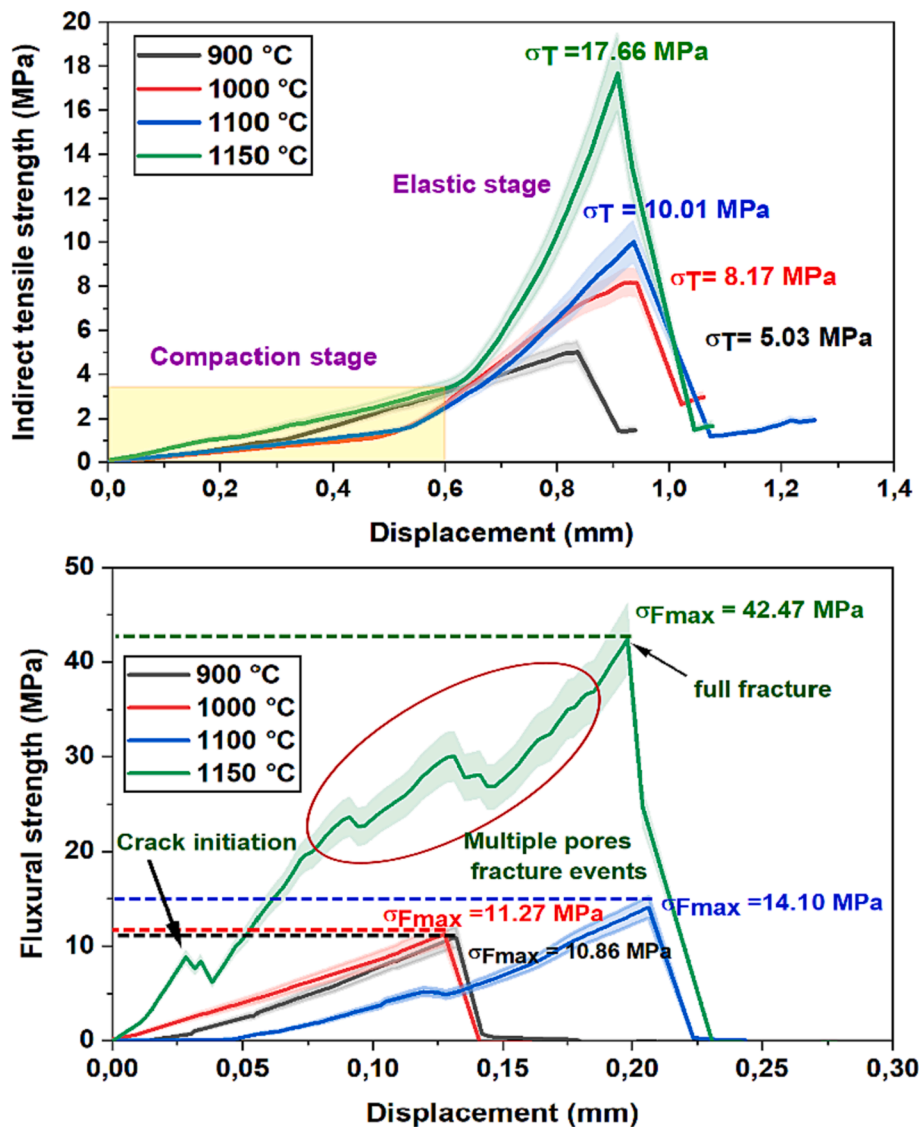


Fig. 10. Indirect tensile and Flexural strengths of fired sample CC.

depicted in Fig. 8) starting from 1100 °C for a duration of 2 h actively supports the augmentation of indirect tensile strength. Pérez-Villarejo et al. (Pérez-Villarejo et al., 2015), in their examination of typical clays and the integration of waste materials into clay bricks, proposed that the elevation in indirect tensile strength within their fired specimens might be ascribed to the decrease in porosity.

3.3.4.2. Relationship between indirect tensile strength and porosity of supports ceramic. Initially, the focus was on exploring the potential associations between mechanical strength, specifically indirect tensile strength, and porosity. This correlation was assessed in the heat-treated specimens of this red clay by employing the Ryshkevitch-Duckworth equation (RYSHKEWITCH, 1953) as indicated by equ (7).

$$\sigma = \sigma_0 \cdot e^{-bp} \quad (7)$$

In this equation, σ denotes the indirect tensile strength and σ_0 signifies the indirect tensile strength when porosity is zero. The constant b stands for the preexponential constant, indicative of the bonding capacity, whereas P is a measure of porosity. This formula has been successfully utilized across an extensive array of porous materials, including but not limited to ceramics. Therefore, porosity is inversely proportional to the logarithm of indirect tensile strength, allowing an

extrapolation of the indirect tensile strength when porosity is zero. In this specific study, the values σ and P were experimentally measured and reported as averages from three separate measures (refer to Fig. 7, 10 and 11). If the parameters σ_0 and b are given, then one can predict the indirect tensile strength for a powdered, fired, compacted specimen. Fig. 12 illustrates the Ryshkevitch-Duckworth graphical interpretation for the CC and NCC samples examined in this study. The observed relationship between open porosity and indirect tensile strength under these experimental conditions is apparent. The resulting straight lines suggest that indirect tensile strength correlates with open porosity. Nevertheless, this correlation is stronger for the NCC sample, as indicated by the higher correlation coefficient ($R^2 = 0.9302$), when compared to the CC sample ($R^2 = 0.9117$). The constant b and indirect tensile strength at zero porosity (σ_0) can be extrapolated from these findings.

To start with, the observed discrepancies from the linear trend in accordance with the Ryshkevitch-Duckworth equation (7) for both CC and NCC samples could be attributed to factors such as irregular shapes, defects, and imperfections related to open pores, as suggested in a prior study (Martínez-Martínez et al., 2022). An essential factor to consider, is the potential existence of closed pores in the fired samples resulting from progressive sintering at elevated temperatures commencing at 1100 °C.

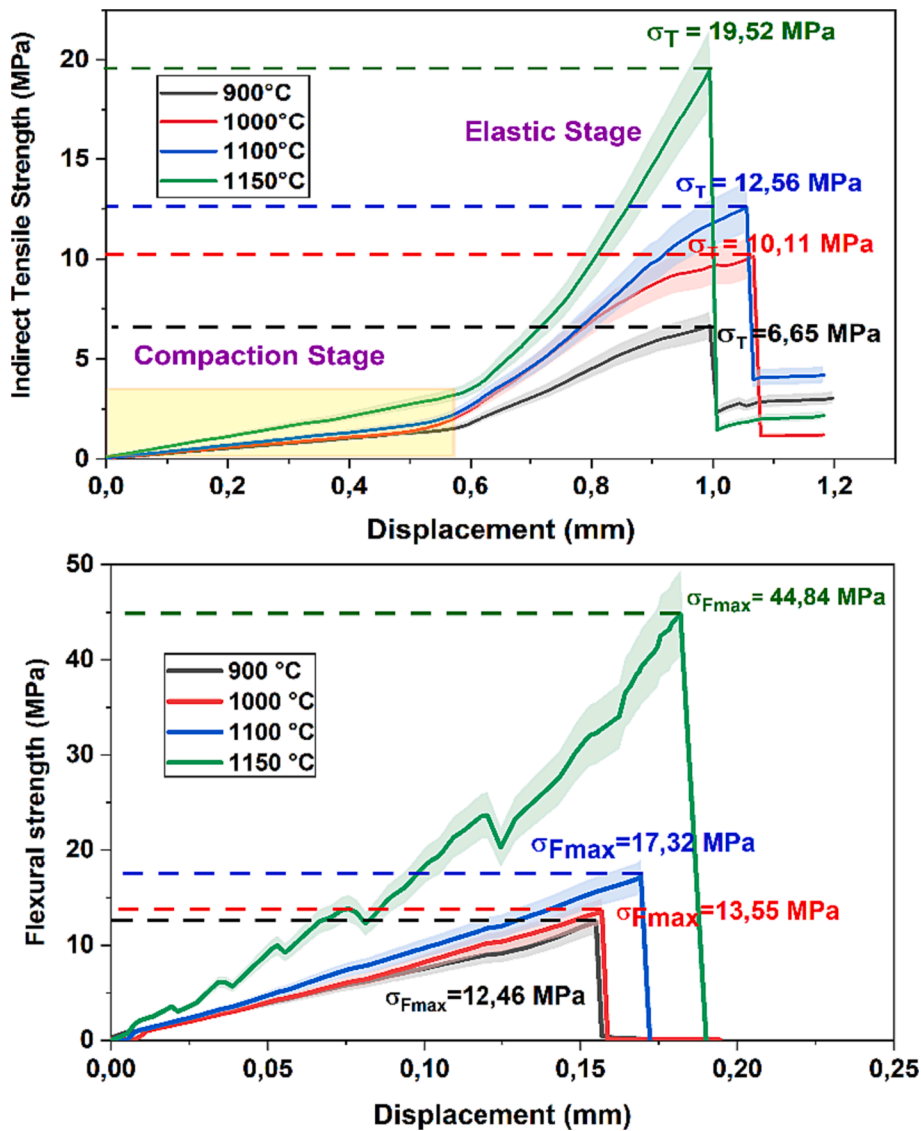


Fig. 11. Indirect tensile and Flexural strengths of fired sample NCC.

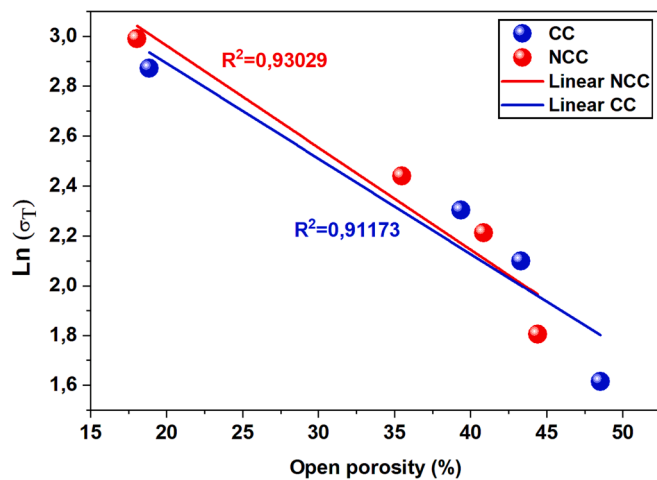


Fig. 12. Relationship between indirect tensile strength (results presented in Figs. 10 and 11) and porosity (Fig. 7) of the samples CC and NCC based on the Ryshkewitch-Duckworth equation.

Such a presence could negatively impact the indirect tensile strength. Indeed, reviewing the indirect tensile strength data featured in Fig. 12 reveals two distinct patterns: (i) the first pattern falls within the 900–1100 °C temperature range (refer to Figs. 10 and 11), where the experimental points cluster, demonstrating a nearly linear relationship between indirect tensile strength and porosity; (ii) the second pattern becomes evident from 1100 to 1150 °C/2h, where a rapid divergence in the values of indirect tensile strength and open porosity can be observed, signaled by a change in the slope of the theoretical straight line (highlighted in Fig. 12). This shift takes place when the fired samples have undergone more extensive sintering (see Figs. 7 and 8). This conclusion is corroborated by the SEM image.

4. Conclusions

The impact of alkaline earth carbonates on the mechanical properties and microstructure of ceramic supports made from Moroccan red clay was investigated, with different firing temperatures (900–1150 °C). By analyzing the results, the main objective of the study was successfully achieved. Table 3 presents a summary of the key findings, including diametric shrinkage, color changes, bulk density, open porosity, water absorption, flexural and indirect tensile strength.

Table 3

Summary of the primary ceramic properties of the Moroccan red clay examined in this study. Firing between 900 and 1150°C.

Ceramic properties	Description
Color	Hematite causes a color shift from red to a deep dark red.
Diametric shrinkage	increased from 1.10 to 9.41 % at 900–1150 °C for CC sample, and increased from 1.04 to 9.20 % at 900–1150 °C for NCC sample.
Water absorption capacity	For CC, decrease from 33.2 % at 900°C to 12.9 % at 1150°C. For NCC, decrease from 31.6 % at 900°C to 12.1 % at 1150 °C.
Bulk density	Increase from 1.39 to 2.01 g/cm ³ at 900–1150 °C for CC, and increase from 1.47 to 2.09 g/cm ³ at 900–1150 °C for NCC.
Open porosity	Decrease from 48.51 to 18.87 % at 900–1150 °C for CC, and decrease from 41.82 to 17.11 % at 900–1150 °C for NCC.
Flexural strength	Increase from 10.86 to 42.47 MPa at 900–1150 °C for CC, and increase from 12.46 to 44.84 MPa at 900–1150 °C for NCC.
Indirect tensile strength	Increase from 5.03 to 17.66 MPa at 900–1150 °C for CC, and increase from 6.65 to 19.52 MPa at 900–1150 °C for NCC. The samples of NCC have a good correlation $R^2 = 0.9303$ compared with CC ($R^2 = 0.9117$) using Ryskhkevitch-Duckworth equation.

At varying firing temperatures, the CC materials exhibit greater weight loss, water absorption, and porosity compared to the NCC materials. This difference is likely attributed to carbonate decomposition and the consequent CO₂ degassing that occurs in the CC materials, while both groups undergo dehydroxylation of clay minerals. Nevertheless, both materials are suitable as ceramic supports, although ceramic supports made from NCC would offer higher quality. As the firing temperature increases, shrinkage also increases, leading to a reduction in water absorption and porosity. This behavior can be attributed to the progressive development of vitrification. These findings highlight the limitations of firing at the highest temperature.

Declaration of competing interest

The authors declare that they have no known competing financial interests or personal relationships that could have appeared to influence the work reported in this paper.

Acknowledgements

This work was supported by the National School of Applied Sciences, Safi, Morocco, and the analysis & characterization center at cadri ayyad university, which are gratefully acknowledged.

References

- Achiou, B., Omari, H.E., Bennazha, J., Albizane, A., Daoudi, L., Saadi, L., Ouammou, M., Younsi, S.A., Maadi, E.A., Chehbouni, M., 2016. Physicochemical and mineralogical characterizations of clays from Fez region (basin of Saiss, Morocco) in the perspective of industrial use. *J. Mater. Environ. Sci.* 7, 1474–1484.
- Achiou, B., Elomari, H., Bouazizi, A., Karim, A., Ouammou, M., Albizane, A., Bennazha, J., Alami Younsi, S., El Amrani, I.E., 2017. Manufacturing of tubular ceramic microfiltration membrane based on natural pozzolan for pretreatment of seawater desalination. *Desalination* 419, 181–187. <https://doi.org/10.1016/j.desal.2017.06.014>.
- Ahmad, T., Guria, C., Mandal, A., 2018a. Optimal synthesis and operation of low-cost polyvinyl chloride/bentonite ultrafiltration membranes for the purification of oilfield produced water. *J. Memb. Sci.* 564, 859–877. <https://doi.org/10.1016/j.memsci.2018.07.093>.
- Ahmad, T., Guria, C., Mandal, A., 2018b. Synthesis, characterization and performance studies of mixed-matrix poly(vinyl chloride)-bentonite ultrafiltration membrane for the treatment of saline oily wastewater. *Process Saf. Environ. Prot.* 116, 703–717. <https://doi.org/10.1016/j.psep.2018.03.033>.
- Arslan, C., Gencel, O., Borazan, I., Sutcu, M., Erdogmus, E., 2021. Effect of waste-based micro cellulose fiber as pore maker on characteristics of fired clay bricks. *Constr. Build. Mater.* 300, 124298. <https://doi.org/10.1016/j.conbuildmat.2021.124298>.
- Arzani, M., Mahdavi, H.R., Sheikhi, M., Mohammadi, T., Bakhtiari, O., 2018. Ceramic monolith as microfiltration membrane: Preparation, characterization and performance evaluation. *Appl. Clay Sci.* 161, 456–463. <https://doi.org/10.1016/j.clay.2018.05.021>.

- Barrouk, I., Alami Younsi, S., Kabbabi, A., Persin, M., Albizane, A., Tahiri, S., 2015. New ceramic membranes from natural Moroccan phosphate for microfiltration application. *Desalin. Water Treat.* 55, 53–60. <https://doi.org/10.1080/19443994.2014.915386>.
- Belibi Belibi, P., Ngumentchouin, M.M.G., Rivallin, M., Ndi Nsami, J., Sieliechi, J., Cerneaux, S., Ngassoum, M.B., Cretin, M., 2015. Microfiltration ceramic membranes from local Cameroonian clay applicable to water treatment. *Ceram. Int.* 41, 2752–2759. <https://doi.org/10.1016/j.ceramint.2014.10.090>.
- Beqqour, D., Achiou, B., Bouazizi, A., Ouaddari, H., Elomari, H., Ouammou, M., Bennazha, J., Alami Younsi, S., 2019. Enhancement of microfiltration performances of pozzolan membrane by incorporation of micronized phosphate and its application for industrial wastewater treatment. *J. Environ. Chem. Eng.* 7, 102981. <https://doi.org/10.1016/j.jece.2019.102981>.
- Bouazizi, A., Saja, S., Achiou, B., Ouammou, M., Calvo, J.I., Aaddane, A., Younsi, S.A., 2016. Elaboration and characterization of a new flat ceramic MF membrane made from natural Moroccan bentonite. Application to treatment of industrial wastewater. *Appl. Clay Sci.* 132–133, 33–40. <https://doi.org/10.1016/j.clay.2016.05.009>.
- Bouzerara, F., Harabi, A., Condom, S., 2009. Porous ceramic membranes prepared from kaolin. *Desalin. Water Treat.* 12, 415–419. <https://doi.org/10.5004/dwt.2009.1051>.
- Cai, J., Xiong, Wang, Y., feng, Xi, X., gang, Li, H., Wei, X., lin, 2015. Using FTIR spectra and pattern recognition for discrimination of tea varieties. *Int. J. Biol. Macromol.* 78, 439–446. <https://doi.org/10.1016/j.ijbiomac.2015.03.025>.
- Cultrone, G., Rodriguez-Navarro, C., Sebastian, E., Cazalla, O., De La Torre, M.J., 2001. Carbonate and silicate phase reactions during ceramic firing. *Eur. J. Mineral.* 13, 621–634. <https://doi.org/10.1127/0935-1221/2001/0013-0621>.
- Dubey, S.P., Sillanpaa, M., Varma, R.S., 2017. Reduction of hexavalent chromium using Sorbaria sorbifolia aqueous leaf extract. *Appl. Sci.* 7. <https://doi.org/10.3390/app7070715>.
- El Ouahabi, M., Daoudi, L., Hatert, F., Fagel, N., 2015. Modified mineral phases during clay ceramic firing. *Clays Clay Miner.* 63, 404–413. <https://doi.org/10.1346/CCMN.2015.0630506>.
- Elomari, H., Achiou, B., Karim, A., Ouammou, M., Albizane, A., Bennazha, J., Alami Younsi, S., Elamrani, I., 2017. Influence of starch content on the properties of low cost microfiltration membranes. *J. Asian Ceram. Soc.* 5, 313–319. <https://doi.org/10.1016/j.jascer.2017.06.004>.
- Faieta-Boada, S.M., McColm, I.J., 1993. Preliminary analysis of the thermal behaviour of an industrially used Ecuadorian clay. *Appl. Clay Sci.* 8, 215–230. [https://doi.org/10.1016/0169-1317\(93\)90039-4](https://doi.org/10.1016/0169-1317(93)90039-4).
- Harrati, A., Manni, A., Hassani, F.O., Sdiri, A., Kalakhi, S.E., Bouari, A.E., Hassani, I.E.E. A.E., Sadik, C., 2022. Potentiality of new dark clay-rich materials for porous ceramic applications in Ouled Sidi Ali Ben Youssef Area (Coastal Meseta, Morocco). *Bol. la Soc. Esp. Ceram. y Vidr.* 61, 130–145. <https://doi.org/10.1016/j.bsecv.2020.08.003>.
- Kakali, G., Perraki, T., Tsivilis, S., Badogiannis, E., 2001. Thermal treatment of kaolin the effect of mineralogy on the pozzolanic activity. *Appl. Clay Sci.* 20, 73–80. [https://doi.org/10.1016/S0169-1317\(01\)00040-0](https://doi.org/10.1016/S0169-1317(01)00040-0).
- Karim, A., Achiou, B., Bouazizi, A., Aaddane, A., Ouammou, M., Bouziane, M., Bennazha, J., Alami Younsi, S., 2018. Development of reduced graphene oxide membrane on flat Moroccan ceramic pozzolan support. Application for soluble dyes removal. *J. Environ. Chem. Eng.* 6, 1475–1485. <https://doi.org/10.1016/j.jece.2018.01.055>.
- Loo, Y.Y., Chieng, B.W., Nishibuchi, M., Radu, S., 2012. Synthesis of silver nanoparticles by using tea leaf extract from Camellia Sinensis. *Int. J. Nanomed.* 7, 4263–4267. <https://doi.org/10.2147/IJN.S33344>.
- Majouli, A., Tahiri, S., Alami Younsi, S., Loukili, H., Albizane, A., 2012. Elaboration of new tubular ceramic membrane from local Moroccan Perlite for microfiltration process. Application to treatment of industrial wastewaters. *Ceram. Int.* 38, 4295–4303. <https://doi.org/10.1016/j.ceramint.2012.02.010>.
- Manni, A., El Haddar, A., El Amrani El Hassani, I.E., El Bouari, A., Sadik, C., 2019. Valorization of coffee waste with Moroccan clay to produce a porous red ceramics (class BIII). *Bol. la Soc. Esp. Ceram. y Vidr.* 58, 211–220. <https://doi.org/10.1016/j.bsecv.2019.03.001>.
- Martínez-Martínez, S., Pérez-Villarejo, L., Garzón, E., Sánchez-Soto, P.J., 2022. Influence of firing temperature on the ceramic properties of illite-chlorite-calcitic clays. *Ceram. Int.* <https://doi.org/10.1016/j.ceramint.2022.11.077>.
- Miyah, Y., Lahrichi, A., Idrissi, M., Anis, K., Kachkoul, R., Idrissi, N., Lairini, S., Nenov, V., Zerrouf, F., 2017. Removal of cationic dye “Crystal Violet” in aqueous solution by the local clay. *J. Mater. Environ. Sci.* 8, 3570–3582.
- Morris, R.V., Golden, D.C., Shelfer, T.D., Lauer, H.V., 1998. Lepidocrocite to maghemite to hematite: a pathway to magnetic and hematitic Martian soil. *Meteorit. Planet. Sci.* 33, 743–751. <https://doi.org/10.1111/j.1945-5100.1998.tb01680.x>.
- Mouïya, M., Abourriche, A., Bouazizi, A., Benhammou, A., El Hafiane, Y., Abouliatim, Y., Nibou, L., Ouammou, M., Ouammou, M., Smith, A., Hannache, H., 2018. Flat ceramic microfiltration membrane based on natural clay and Moroccan phosphate for desalination and industrial wastewater treatment. *Desalination* 427, 42–50. <https://doi.org/10.1016/j.desal.2017.11.005>.
- Mouïya, M., Arib, A., Taha, Y., Tamraoui, Y., Hakkou, R., Alami, J., Huger, M., Tessier-Doyen, N., 2022. Characterization of a chistolite-type andalusite: structure and physicochemical properties related to mullite transformation. *Mater. Res. Express* 9. <https://doi.org/10.1088/2053-1591/ac81a2>.
- Mudrinić, T., Mojović, Z., Milutinović-Nikolić, A., Mojović, M., Žunić, M., Vukelić, N., Jovanović, D., 2015. Electrochemical activity of iron in acid treated bentonite and influence of added nickel. *Appl. Surf. Sci.* 353, 1037–1045. <https://doi.org/10.1016/j.apsusc.2015.07.054>.
- Ngayakamo, B.H., Bello, A., Onwualu, A.P., 2020. Development of eco-friendly fired clay bricks incorporated with granite and eggshell wastes. *Environ. Challenges* 1, 100006. <https://doi.org/10.1016/j.envc.2020.100006>.

- Njeumen Nkayem, D.E., Mbey, J.A., Kenne Diffo, B.B., Njopwouo, D., 2016. Preliminary study on the use of corn cob as pore forming agent in lightweight clay bricks: Physical and mechanical features. *J. Build. Eng.* 5, 254–259. <https://doi.org/10.1016/j.jobbe.2016.01.006>.
- Pérez-Villarejo, L., Martínez-Martínez, S., Carrasco-Hurtado, B., Eliche-Quesada, D., Ureña-Nieto, C., Sánchez-Soto, P.J., 2015. Valorization and inertization of galvanic sludge waste in clay bricks. *Appl. Clay Sci.* 105–106, 89–99. <https://doi.org/10.1016/j.clay.2014.12.022>.
- Raigón-Pichardo, M., García-Ramos, G., Sánchez-Soto, P.J., 1996. Characterization of a waste washing solid product of mining granitic tin-bearing sands and its application as ceramic raw material. *Resour. Conserv. Recycl.* 17, 109–124. [https://doi.org/10.1016/0921-3449\(96\)01108-1](https://doi.org/10.1016/0921-3449(96)01108-1).
- Rakcho, Y., Mouiya, M., Bouazizi, A., Abouliatim, Y., Sehaqui, H., Mansouri, S., Benhammou, A., Hannache, H., Alami, J., Abourriche, A., 2023. Treatment of seawater and wastewater using a novel low-cost ceramic membrane fabricated with red clay and tea waste. *Arab. J. Chem.* 16, 105277 <https://doi.org/10.1016/j.arabjc.2023.105277>.
- Rodrigues, R., Mierzwa, J.C., Vecitis, C.D., 2019. Mixed matrix polysulfone/clay nanoparticles ultrafiltration membranes for water treatment. *J. Water Process Eng.* 31 <https://doi.org/10.1016/j.jwpe.2019.100788>.
- RYSHKEWITCH, E., 1953. Compression Strength of Porous Sintered Alumina and Zirconia. *J. Am. Ceram. Soc.* 36, 65–68. <https://doi.org/10.1111/j.1151-2916.1953.tb12837.x>.
- Saif, S., Tahir, A., Asim, T., Chen, Y., 2016. Plant mediated green synthesis of CuO nanoparticles: Comparison of toxicity of engineered and plant mediated CuO nanoparticles towards *Daphnia magna*. *Nanomaterials* 6, 1–15. <https://doi.org/10.3390/nano6110205>.
- Sanchez-Soto, P.J., Perez-Rodriguez, J.L., 1989. SEM study of pyrophyllite high-temperature transformations. *J. Mater. Sci.* 24, 3774–3778. <https://doi.org/10.1007/BF02385769>.
- Semiz, B., 2017. Characteristics of clay-rich raw materials for ceramic applications in Denizli region (Western Anatolia). *Appl. Clay Sci.* 137, 83–93. <https://doi.org/10.1016/j.clay.2016.12.014>.
- Senthilkumar, S.R., Sivakumar, T., 2014. Green tea (*Camellia sinensis*) mediated synthesis of zinc oxide (ZnO) nanoparticles and studies on their antimicrobial activities. *Int. J. Pharm. Pharm. Sci.* 6, 461–465.
- Teklay, A., Bojer, M., Adelsward, A., Yin, C., Rosendahl, L., 2014. Simulation of flash dehydroxylation of clay particle using gPROMS: A move towards green concrete. *Energy Procedia* 61, 556–559. <https://doi.org/10.1016/j.egypro.2014.11.1169>.
- Thuc, C.N.H., Grillet, A.C., Reinert, L., Ohashi, F., Thuc, H.H., Duclaux, L., 2010. Separation and purification of montmorillonite and polyethylene oxide modified montmorillonite from Vietnamese bentonites. *Appl. Clay Sci.* 49, 229–238. <https://doi.org/10.1016/j.clay.2010.05.011>.
- Vizcayno, C., de Gutiérrez, R.M., Castello, R., Rodriguez, E., Guerrero, C.E., 2010. Pozzolan obtained by mechanochemical and thermal treatments of kaolin. *Appl. Clay Sci.* 49, 405–413. <https://doi.org/10.1016/j.clay.2009.09.008>.
- Weng, X., Huang, L., Chen, Z., Megharaj, M., Naidu, R., 2013. Synthesis of iron-based nanoparticles by green tea extract and their degradation of malachite. *Ind. Crops Prod.* 51, 342–347. <https://doi.org/10.1016/j.indcrop.2013.09.024>.